Tuning edge localized spin waves in magnetic microstripes by proximate magnetic structures

Zhizhi Zhang[1,2], Michael Vogel[1], M. Benjamin Jungfleisch[3], Axel Hoffmann[1,4], Yan Nie[2,*], and Valentine Novosad[1,†]

[1]Materials Science Division, Argonne National Laboratory, Lemont, IL 60439, USA
[2]School of Optical & Electronic Information, Huazhong University of Science and Technology, Wuhan 430074, China
[3]Department of Physics & Astronomy, University of Delaware, Newark, DE 19716, USA
[4]Department of Materials Science and Engineering, University of Illinois at Urbana-Champaign, Urbana, IL 61801, USA

Abstract

The propagation of edge localized spin waves (E-SWs) in yttrium iron garnet (YIG, $Y_3Fe_5O_{12}$) microstripes with and without magnetic microstructures in close proximity is investigated by micromagnetic simulations. A splitting of the dispersion curve with the presence of permalloy (Py; $Ni_{81}Fe_{19}$) stripe is observed. The results show that E-SWs on the two edges of YIG stripe have different wavelengths, group velocities, and decay lengths at the same frequencies. The role of the Py stripe was found to be the source of the inhomogeneous static dipolar field without dynamic coupling with YIG. This work opens new perspectives for the design of innovative spin wave interference-based logic devices.

Introduction

Data transmission with spin waves (SWs) and their particle-like analog, magnons, is a promising direction for next generation information devices because of their low heat dissipation and high efficiency [1-5]. One potentially important application of SWs is logic functionality based on the interaction of waves, especially on the wave interference [6-10]. Therefore, the SWs need to be wave vector monochromatic and well localized. Under this prerequisite, several works have studied SWs propagating in domain walls [11-13]. One restriction of this approach is that the frequencies of such SWs are lower than their counterparts within the domains themselves. Thus, there are additional opportunities for exploring SW propagation in patterned microstripes with eigen frequencies in the GHz range exceeding the limit for SW propagation guided by domain wall structures. There are two kinds of SWs in such structures: waveguide SWs (W-SWs) and edge localized SWs (E-SWs). While the W-SWs contain a set of multiple modes with various wave vectors hybridized in the central region of the microstripes [14-16], the E-SWs' confined in narrow channels along the edges of the sample and possess a monochromatic wave vector [17-20]. Identifying an effective method for manipulating the propagation of E-SWs is an important step towards the successful development of spin wave-based magnonic devices [21].

In this work, we studied the propagation of the E-SWs in yttrium iron garnet (YIG; $Y_3Fe_5O_{12}$) stripes with and without laterally proximate permalloy (Py; $Ni_{81}Fe_{19}$) stripes close to one edge. YIG has the lowest known magnetic damping factor (α) and lower

magnetization saturation (M_s) compared with the metal material [22]. Py was selected for its high M_s, which is almost six times larger than M_s of YIG, while α still maintains a low value. We calculate dispersion diagrams of the SWs in the waveguides and quantitatively analyzed the E-SWs in YIG stripes, including the wavelengths (λ), decay lengths (δ), and group velocities (v_g) at certain frequencies. Furthermore, the effects of the Py stripe on the E-SWs in YIG stripe are fully explored, and the mechanisms of these effects are discussed, potentially leading to implications for future engineering applications.

Methods

We performed micromagnetic simulations on SWs propagating in magnetic thin-film microstrips using the MuMax3 software [23]. Fig. 1 (a) shows the schematic of the studied model: a 10 μm × 1 μm × 50 nm YIG microstripe and a Py stripe with the same sizes laterally close to one edge (referred here as YIG/Py structure). The gap between the edges d_{gap} was first fixed at 100 nm. An external magnetic field (H_{ext}) of 1000 Oe in the y-direction was applied to the structure, corresponding to the Damon-Eschbach (DE) geometry [24]. Material parameters used in the simulation were $4\pi M_s$ = 1860 G, exchange constant A_{ex}= 4×10^{-7} erg/cm, and $\alpha = 7.561\times10^{-4}$ for YIG [25] and $4\pi M_s = 1.08\times10^5$ G, A_{ex}= 1.3×10^{-6} erg/cm, α=0.01 for Py. In addition, the attenuating areas (4 μm on each end, not shown here) with α gradually increased to 0.25 and served as absorption boundaries to avoid the reflection at the ends of the stripes, thus effectively simulate the case of infinitely long stripes.

To analyze the dispersion relations of the propagating SWs in the magnetic stripes, the excitations were applied locally in the antenna area using a sinc function $h_x = h_0 \frac{\sin\left(2\pi f_c\left(t-t_0\right)\right)}{2\pi f_c\left(t-t_0\right)}$ [26] with a cut off frequency f_c = 50 GHz [Fig. 1 (b)] and h_0 = 10 Oe. f_c was high enough to satisfy the SW propagating conditions of both YIG and Py, and the h_0 was low enough to avoid any nonlinear effects.[27] Fig. 1(b) shows the sinc excitation in the time domain, which has a pulse-like shape. The frequency spectrum obtained by fast Fourier transform (FFT) shown in Fig. 1 (c) indicates that such kind of excitation has a uniform intensity in the whole frequency band under f_c and zero intensity above f_c. The total simulation time was 200 ns, and the results recorded the dynamic normalized magnetization (m_z/M_s) evolution as a function of time and position along the YIG stripe. Therefore, m_z/M_s became a two-dimensional matrix $m_z/M_s(x, t)$. The dispersion relations were obtained through the two-dimensional FFT (2D-FFT) operation on $m_z/M_s(x, t)$.[28] Subsequently, continuous sine excitations with specific frequencies were applied continuously to study the detailed SW properties (λ, v_g and δ). H_{eff}, which includes contributions from the external magnetic field (H_{ext}), dipolar fields, and short-range exchange interactions, is extracted from the simulation and was used for further analysis, as shown below.

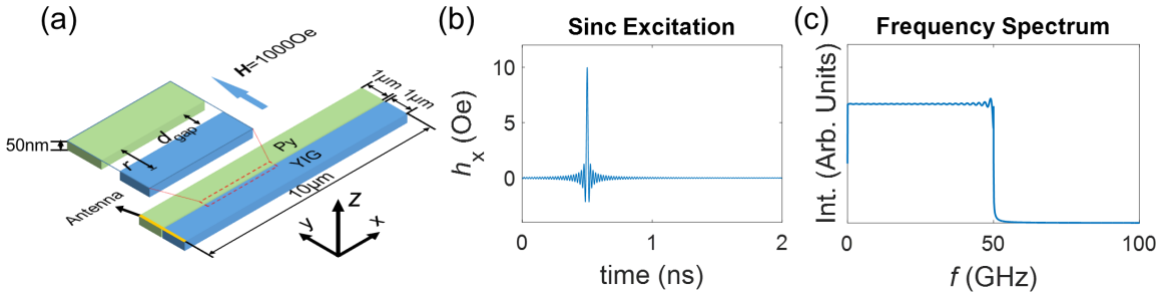

Fig. 1 (a) Schematic of the proposed YIG/Py structures. The gap between the edges is d_{gap} = 100 nm, and the distance from any in-plane point to the edge of the Py stripe is r. The yellow antenna region indicates the SW generation. (b) Temporal evolution of sinc function field with h_0 = 10 Oe applied along x-axis with a Gaussian distribution centered in yellow antenna region. (c) Frequency spectrum obtained from FFT of applied sinc field with f_c = 50 GHz.

Discussion

The dispersion diagrams of the single YIG and the YIG and Py stripes in YIG/Py are shown in Fig. 2 (a), (b), and (c), respectively. In all stripes, there clearly exists a set of hybridized W-SWs localized in the higher frequency band and E-SWs in a lower frequency band. According to Ref. [29], the SWs dispersion relation of the DE geometry in lossless materials can be theoretically written as

$$f = \sqrt{\left(f_0 + \lambda_{ex}^{\,2} f_M k^2\right)\left(f_0 + \lambda_{ex}^{\,2} f_M k^2 + f_M\right) + \frac{f_M^{\,2}}{4}\left(1 - e^{-2kd}\right)} \qquad (1)$$

where $f_0 = \gamma H_0$, $f_M = \gamma(4\pi M_s)$, d is the thickness of the film, k is the wave vector, γ is the gyromagnetic ratio (2.8 MHz/Oe), and λ_{ex} is the exchange length and is equal to $\sqrt{A_{ex}/2\pi M_s^{\,2}}$ (in CGS)[30]. The formation of E-SWs is due to the prominently reduced H_{eff} at the edges by the demagnetization field, leading to the lower frequencies than those of W-SWs[31]. In addition, the E-SWs on the two edges of a single YIG stripe have a degenerated dispersion curve because of the symmetric magnetic configurations. In contrast, the degenerated states were split into two curves for the YIG/Py structure, as shown in Fig. 2 (b), due to the asymmetric presence of Py. The W-SW dispersion curves in YIG microstripe are also further separated with the presence of Py. Because of the much higher M_s of Py compared to YIG, the SWs in Py stripe propagate at significantly higher frequencies (above 6 GHz) than those of YIG (mostly lower than 6 GHz) under the same H_{ext}, as shown in Fig. 2 (c) and in accordance with Eq. (1).

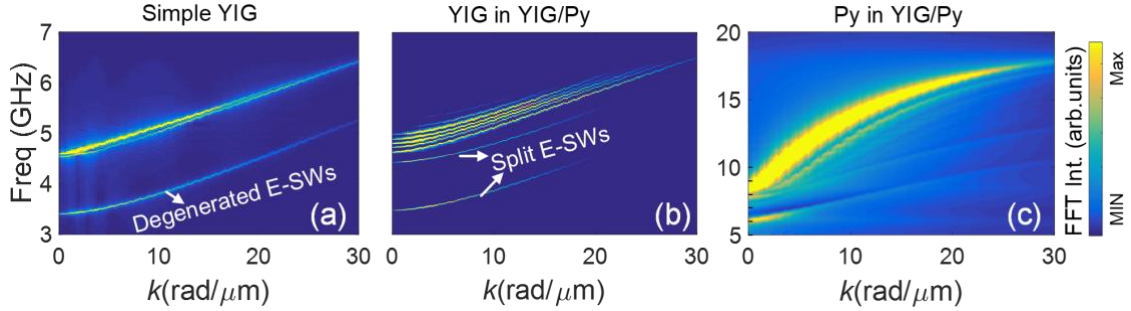

Fig. 2 Dispersion relations for both W-SWs and E-SWs propagating in (a) single YIG stripe without Py stripe, (b) YIG stripe in YIG/Py, and (c) Py stripe in YIG/Py. k is along the x-axis.

The dispersion diagrams of YIG stripes without and with the proximate Py stripe were zoomed in for further analysis, as shown in Fig. 3 (a) and (b), respectively. To study the detailed behaviors of the E-SWs propagating on the two edges of YIG stripes, we applied a continuous excitation of the sine function $h_x = h_0\sin(2\pi ft)$ in the antenna region with $f = 3.9$ and 4.5 GHz, respectively. Here, $h_0 = 1$ Oe is weak enough to avoid nonlinear effects [27]. The total simulation time was 80 ns to ensure that the system reaches a steady state. To obtain the accurate values of λ and δ, we fit the m_z/M_s space distributions in steady state (t = 80 ns) using the following equation:

$$\frac{m_z}{M_s} = A\sin\left(\frac{2\pi}{\lambda}x+\theta\right)\exp\left(-\frac{x}{\delta}\right) \quad (2)$$

where θ is a phase factor and A is a scaling factor. The v_g of every E-SW was determined using l/τ, where l is the length of the stripe, equal to 10 μm, and τ is the time for the m_z/M_s at the right end reaching the stable state [see Fig. 3 (f)]. Fig. 3 (c) and (d) show the m_z/M_s of the single YIG and the YIG in YIG/Py on both edges at t=80 ns under the 3.9-GHz excitation. These figures indicate that the 3.9-GHz E-SWs propagate on both edges of the single YIG stripe with the same λ, δ, and v_g (Supplementary Movie 1[32]). In contrast, these E-SWs can propagate only on the edge farther away from Py in the YIG stripe. On the edge closer to Py, the oscillation of the m_z/M_s was confined near the excitation (Supplementary Movie 2 [32]). The 4.5-GHz E-SWs can propagate on both edges of the YIG stipe in YIG/Py, as shown in Fig. 3 (e), but with different λ, δ, and v_g (Supplementary Movie 3[32]). The time evolution of m_z/M_s shown in Fig. 3 (f) indicates that the SWs propagation process includes the transient state (yellow region) and the steady state (green region).

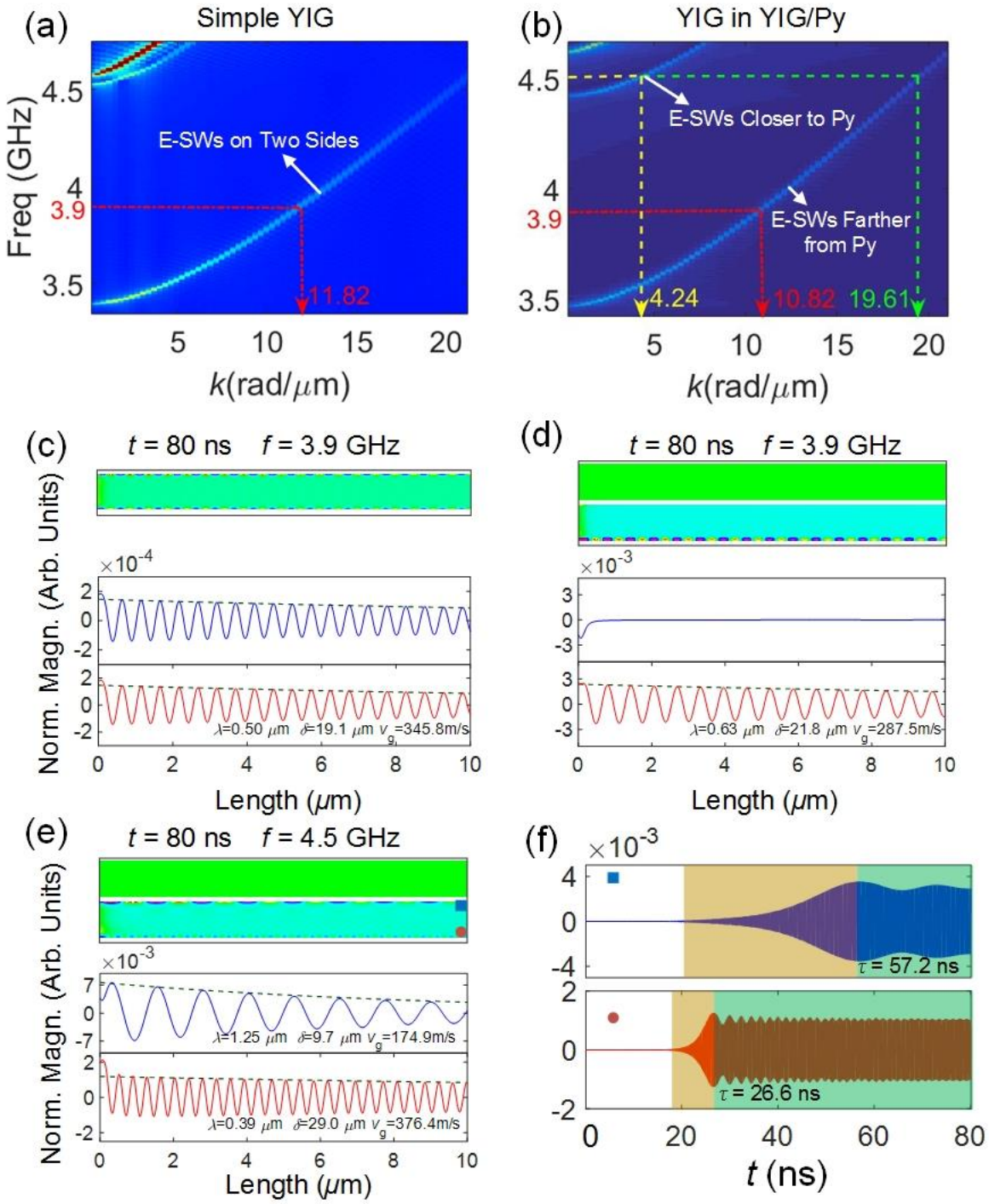

Fig. 3 Zoomed in dispersion diagram focused on E-SWs in (a) single YIG and (b) YIG stripe in YIG/Py. The dashed lines depict the wave vectors for specific excitation frequencies. The response of the m_z/M_s in (c) single YIG, (d) YIG stripe in YIG/Py at t = 80 ns under 3.9-GHz excitation and (e) YIG stripe in YIG/Py at t = 80 ns under 4.5-GHz excitation. Upper panels are the global 2D maps of the m_z/M_s intensity (Green represents Py, same hereinafter); lower panels are the m_z/M_s intensity distribution along the two edges of YIG stripes, where the blue curves are for the edge closer to Py, the red curves are for the edge far away from Py, and the green dash curves are the envelop line obtained from the fitting. (f) The temporal evolution of m_z/M_s monitored at the ends of the two edges of the YIG stripe in the case of (e). Blue

square and red circle dots represent the positions (10 μm away from the excitation) shown in the upper panel of (e). The yellow patch in the plot indicates the transient states, and the green patch indicates the stable states. τ is the time for the m_z/M_s at the positions reaching to the stable state.

In order to better understand the striking difference of the E-SWs propagating along the two edges of the YIG stripe in YIG/Py, the impacts of the proximate Py on the YIG stripe were inspected by focusing on two different aspects: the static H_{eff} effect because of the presence of Py and the dynamic coupling effect between YIG and Py.

H_{eff} is determined from the micromagnetic simulations across a single YIG stripe under the 1000 Oe applied field without microwave excitation and is shown in Fig. 4 (a). The figure shows that the H_{eff} distribution has the following features: 1. Because of the demagnetizing field distributed at the edges of the stripe, the H_{eff} is weaker than the applied field; 2. Inside the YIG stripe, the H_{eff} reduces significantly close to the edges, creating the SW potential wells[33], where the dynamic magnetization is confined similar to the localization of quantum particles in potential wells; 3. The SW potential wells in the two edges of the single YIG stripe have a symmetric profile because of the symmetric geometry of the magnetic system. In contrast, the static H_{eff} distributions in YIG and Py stripes in YIG/Py shown in Fig. 4 (b) indicate the profile is significantly changed by the magnetic dipoles in Py. The depths and positions of the SW potential wells on the two edges of single YIG (from 320 to 970 Oe) are similar with those (from 340 to 930 Oe) on the edge farther away from Py of the YIG in YIG/Py. The increase of H_{eff} leads to a splitting of the dispersion curve by a shift toward the higher frequency bands. This agrees with the predictions given by Eq. (1) and the positions of E-SWs dispersion curves in Fig. 2 (a) and (b). It also results in the increase of λ[34, 35] and the decrease of v_g and δ[36], agreeing with the results in Fig. 3.

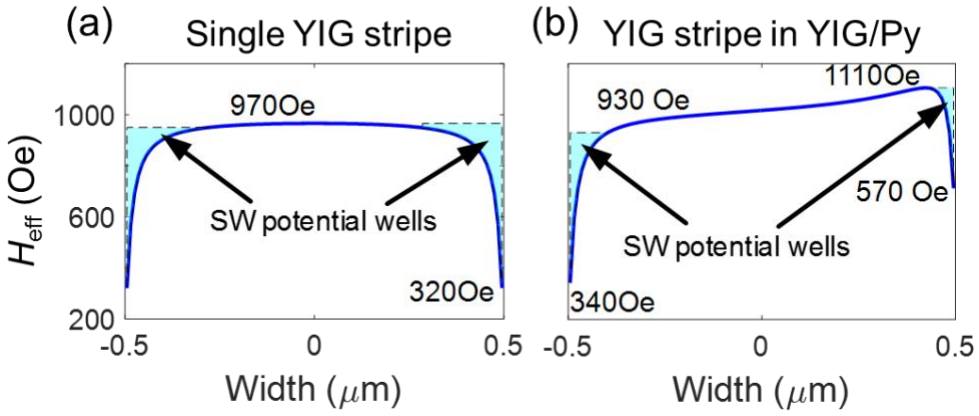

Fig. 4 The y-component of H_{eff} across (a) single YIG stripe and (b) YIG stripe and Py stripe in YIG/Py under 1000 Oe.

To quantitatively analyze the additional field introduced by Py, we numerically calculated the dipolar field induced by Py stripe ($H_{dip\text{-}Py}$), as shown in Fig. 5 (a), and fitted it using the following equation:

$$H_{fit} = \frac{a}{r^n} + b \qquad (3)$$

where a is a real scaling parameter, b is an offset, r is the distance from any in-plane

point to the edge of the Py stripe as shown in Fig. 1(a), and n is the coefficient to be determined. $H_{\text{dip-Py}}$ was found to be proportional to $1/r$, whose intensity was about 280 Oe at r = 0.1 μm and reduced rapidly to 20 Oe at r = 1.1 μm. For further comparison, the dispersion relations of the YIG stripe in YIG/Py with d_{gap} = 200 and 1000 nm were numerically calculated respectively, as shown in Fig. 5 (b) and (c), respectively. We noticed that the curves of the E-SWs dispersions were getting closer with the increasing of the gap distance compared with Fig. 2(b), and finally, they almost merged together at d_{gap} = 1000 nm, where the $H_{\text{dip-Py}}$ decayed to nearly zero. In addition, when comparing Fig. 4 (a) and Fig. 4 (b), we notice a gradient of H_{eff} appears in the middle of YIG stripe with the presence of Py. The homogeneity of H_{eff} in the middle of the YIG stripe is also broken by $H_{\text{dip-Py}}$. The separating degrees of the W-SW dispersion curves are also weakened with the increase of d_{gap}, as shown in Fig. 2 (b), Fig. 5 (b) and (c). In a brief summary, the results show that the static $H_{\text{dip-Py}}$ introduced by Py was one factor resulting in the difference of the E-SWs propagating on the two edges of the YIG stripe in YIG/Py.

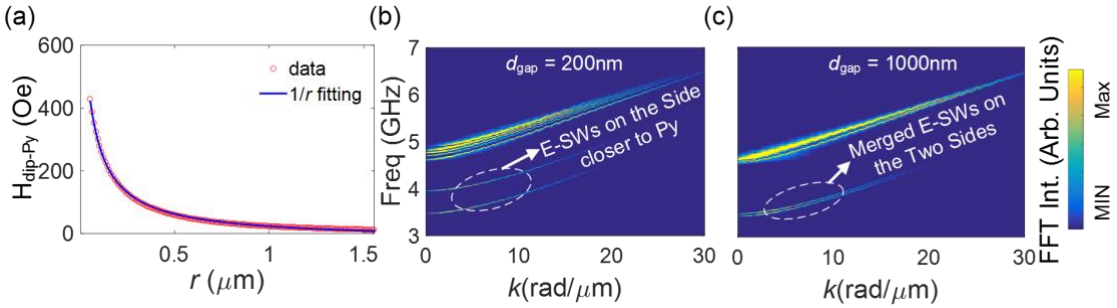

Fig. 5 (a) Profile of the y-component $H_{\text{dip-Py}}$ versus the distance to the fully magnetized Py stripe. (b) The dispersion relations of the SWs propagating in YIG stipes in YIG/Py with d_{gap} = 200 and 1000 nm, respectively.

If the two magnetic structures are close to each other, dynamic coupling might occur. Dynamic coupling means that the dynamic magnetization transfers repeatedly between one structure and the other, resulting in the splitting of the dispersion curves[5]. The dynamic coupling has been observed in two YIG stripes horizontally close to each other[5, 37-39] and multiple vertical layers with different materials[40-44]. In those cases, the frequencies of the SWs in different magnetic structures overlapped with each other under certain conditions. In our case, according to the dispersion relations shown in Fig. 2(b) and (c), the frequencies of the propagating E-SWs in YIG and Py are not overlapping. Therefore, no dynamic coupling occurred during the propagation of the studied E-SWs. To further confirm this point, we perform a simulation on the single YIG stripe under 4.5 GHz excitation. The static external field was set as the superposition of the 1000 Oe homogeneous field and the inhomogeneous field described by Eq. (3) with n = 1 in the width direction. The 2D maps of the m_z/M_s intensity in YIG stripe and the temporal evolution of m_z/M_s on the two edges at the end of the YIG stripe are shown in Fig. 6 (a) and (b), respectively. The E-SWs in this case showed the same behaviors as those shown in Fig. 3 (e) and (f). Consequently, the role of Py stripe is simply a source of an additional inhomogeneous magnetic field without dynamic coupling with YIG.

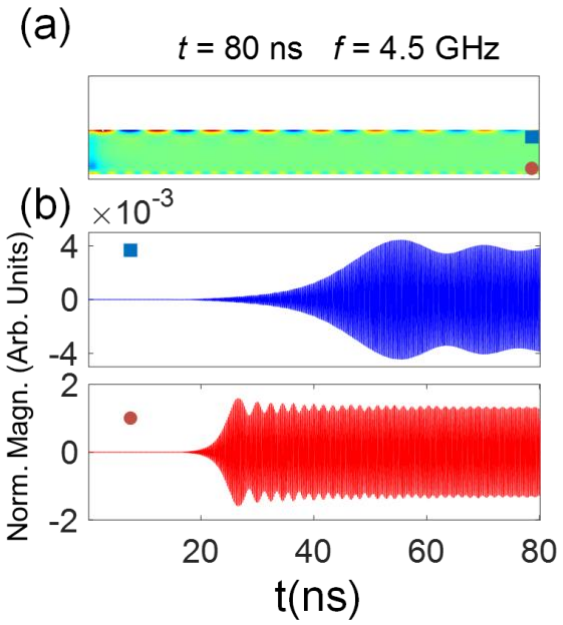

Fig. 6 (a) 2D maps of the m_z/M_s intensity of the YIG stripe (f = 4.5 GHz and t = 80 ns) under the static external field consisting of the 1000 Oe homogeneous field and the inhomogeneous field aligned perpendicular to the long side of the stripe, as described by Eq. (3) with n = 1. (b) The temporal evolution of m_z/M_s monitored at the end of the YIG stripe. Blue square and red circle dots represent the corresponding positions shown in (a).

Here, by tuning the position of the dispersion curve in the diagram, the SWs can propagate with designed properties in two separated channels in just one waveguide. In addition, the induced static dipolar field is an essential factor for tuning the dispersion curves that strongly depends on the magnetization of the proximate magnet. Consequently, we can expect to actively tune the E-SWs by changing the magnetization, for example, the temperature of the proximate Py stripe can be controlled by applying the charge current. The Joule heat changes the magnetization as well as the induced dipolar field. Such performances indicate a method toward producing novel magnonic devices.

Conclusion

In summary, we studied the E-SWs propagating behaviors on the two edges of the YIG stripe with and without the laterally proximate Py stripe. The degenerated dispersion curve of the E-SWs in YIG stripe was separated into two curves with the presence of the Py stripe. Correspondingly, the E-SWs on the two edges of YIG stripe have different λ, v_g, and δ at the same frequencies. The reasons for the splitting of the dispersion curve were investigated through exploring the role Py played in the magnetic structure. The additional Py stripe acts as a source of the inhomogeneous magnetic field. No dynamic coupling occurred between YIG and Py in the structure. The results show the unique characteristics of SWs integrated in a single waveguide. Since the phase difference between the SWs is related to their wavelengths, the structure opens new perspectives for the design of innovative logic elements based on constructive or destructive SW interference.

Acknowledgment

Work at Argonne was supported by the U. S. Department of Energy, Office of Science, Materials Science and Engineering Division. Z Z acknowledges the financial support of China Scholarship Council (no. 201706160146). M B J acknowledges support from the US National Science Foundation under Grant No. 1833000. The authors thank Prof. Andrii V. Chumak, Prof. Paul A. Crowell and Dr. Yi Li for constructive discussions.

*nieyan@hust.edu.cn
†novosad@anl.gov

References

1. Chumak, A.V., et al., *Magnon spintronics.* Nature Physics, 2015. **11**(6).
2. Krawczyk, M. and D. Grundler, *Review and prospects of magnonic crystals and devices with reprogrammable band structure.* Journal of Physics: Condensed Matter, 2014. **26**(12): p. 123202.
3. Chumak, A.V., A.A. Serga, and B. Hillebrands, *Magnon transistor for all-magnon data processing.* Nature Communications, 2014. **5**: p. 4700.
4. Haldar, A., D. Kumar, and A.O. Adeyeye, *A reconfigurable waveguide for energy-efficient transmission and local manipulation of information in a nanomagnetic device.* Nat Nano, 2016. **11**(5): p. 437-443.
5. Wang, Q., et al., *Reconfigurable nanoscale spin-wave directional coupler.* Science Advances, 2018. **4**(1).
6. Schneider, T., et al., *Realization of spin-wave logic gates.* Applied Physics Letters, 2008. **92**(2): p. 022505.
7. Nikitin, A.A., et al., *A spin-wave logic gate based on a width-modulated dynamic magnonic crystal.* Applied Physics Letters, 2015. **106**(10): p. 102405.
8. Fischer, T., et al., *Experimental prototype of a spin-wave majority gate.* Applied Physics Letters, 2017. **110**(15): p. 152401.
9. Klingler, S., et al., *Design of a spin-wave majority gate employing mode selection.* Applied Physics Letters, 2014. **105**(15): p. 152410.
10. Hertel, R., W. Wulfhekel, and J. Kirschner, *Domain-Wall Induced Phase Shifts in Spin Waves.* Physical Review Letters, 2004. **93**(25): p. 257202.
11. Wagner, K., et al., *Magnetic domain walls as reconfigurable spin-wave nanochannels.* Nature Nanotechnology, 2016. **11**: p. 432.
12. Albisetti, E., et al., *Nanoscale spin-wave circuits based on engineered reconfigurable spin-textures.* Communications Physics, 2018. **1**(1): p. 56.
13. Sluka, V., et al., *Emission and propagation of 1D and 2D spin waves with nanoscale wavelengths in anisotropic spin textures.* Nature Nanotechnology, 2019. **14**(4): p. 328-333.
14. Demidov, V.E., et al., *Self-focusing of spin waves in Permalloy microstripes*. Applied Physics Letters, 2007. **91**(25): p. 252504.
15. Demidov, V.E., et al., *Mode interference and periodic self-focusing of spin waves in permalloy microstripes.* Physical Review B, 2008. **77**(6): p. 064406.

16. Pirro, P., et al., *Interference of coherent spin waves in micron-sized ferromagnetic waveguides.* phys. stat. solidi (b), 2011. **248**(10): p. 2404-2408.
17. Pirro, P., et al., *Spin-wave excitation and propagation in microstructured waveguides of yttrium iron garnet/Pt bilayers.* Applied Physics Letters, 2014. **104**(1): p. 012402.
18. Sebastian, T., et al., *Nonlinear Emission of Spin-Wave Caustics from an Edge Mode of a Microstructured $Co_2Mn_{0.6}Fe_{0.4}Si$ Waveguide.* Physical Review Letters, 2013. **110**(6): p. 067201.
19. Park, J.P., et al., *Spatially Resolved Dynamics of Localized Spin-Wave Modes in Ferromagnetic Wires.* Physical Review Letters, 2002. **89**(27): p. 277201.
20. Bayer, C., et al., *Spin waves in an inhomogeneously magnetized stripe.* Physical Review B, 2004. **69**(13): p. 134401.
21. Lara, A., et al., *Information processing in patterned magnetic nanostructures with edge spin waves.* Scientific Reports, 2017. **7**(1): p. 5597.
22. Serga, A.A., A.V. Chumak, and B. Hillebrands, *YIG magnonics.* Journal of Physics D: Applied Physics, 2010. **43**(26): p. 264002.
23. Vansteenkiste, A., et al., *The design and verification of MuMax3.* AIP Advances, 2014. **4**(10): p. 107133.
24. Damon, R.W. and J.R. Eshbach, *Magnetostatic modes of a ferromagnet slab.* Journal of Physics and Chemistry of Solids, 1961. **19**(3): p. 308-320.
25. Li, S., et al., *Epitaxial patterning of nanometer-thick $Y_3Fe_5O_{12}$ films with low magnetic damping.* Nanoscale, 2016. **8**(1): p. 388-394.
26. Lee, K.-S., D.-S. Han, and S.-K. Kim, *Physical Origin and Generic Control of Magnonic Band Gaps of Dipole-Exchange Spin Waves in Width-Modulated Nanostrip Waveguides.* Physical Review Letters, 2009. **102**(12): p. 127202.
27. Livesey, K., *Chapter 4 - Nonlinear Behavior in Metallic Thin Films and Nanostructures*, in *Handbook of Surface Science*, R.E. Camley, Z. Celinski, and R.L. Stamps, Editors. 2015, North-Holland. p. 169-214.
28. Kumar, D., et al., *Numerical calculation of spin wave dispersions in magnetic nanostructures.* Journal of Physics D: Applied Physics, 2011. **45**(1): p. 015001.
29. Kalinikos, B.A. and A.N. Slavin, *Theory of dipole-exchange spin wave spectrum for ferromagnetic films with mixed exchange boundary conditions.* Journal of Physics C: Solid State Physics, 1986. **19**(35): p. 7013.
30. Abo, G.S., et al., *Definition of Magnetic Exchange Length.* IEEE Transactions on Magnetics, 2013. **49**(8): p. 4937-4939.
31. Gubbiotti, G., et al., *Magnetic field dependence of quantized and localized spin wave modes in thin rectangular magnetic dots.* Journal of Physics: Condensed Matter, 2004. **16**(43): p. 7709.
32. See Supplemental Material at [URL will be inserted by publisher] for three movie files and one file for more detailed descriptions.
33. Jorzick, J., et al., *Spin Wave Wells in Nonellipsoidal Micrometer Size Magnetic Elements.* Physical Review Letters, 2002. **88**(4): p. 047204.
34. Vogt, K., et al., *All-optical detection of phase fronts of propagating spin waves in a Ni81Fe19 microstripe.* Applied Physics Letters, 2009. **95**(18): p. 182508.
35. Demidov, V.E., S. Urazhdin, and S.O. Demokritov, *Control of spin-wave phase and*

wavelength by electric current on the microscopic scale. Applied Physics Letters, 2009. **95**(26): p. 262509.
36. Stancil, D.D. and A. Prabhakar, *Spin waves*. 2009: Springer.
37. Sadovnikov, A., et al., *Directional multimode coupler for planar magnonics: Side-coupled magnetic stripes.* Applied Physics Letters, 2015. **107**(20): p. 202405.
38. Sadovnikov, A., et al., *Nonlinear spin wave coupling in adjacent magnonic crystals.* Applied Physics Letters, 2016. **109**(4): p. 042407.
39. Sadovnikov, A.V., et al., *Voltage-Controlled Spin-Wave Coupling in Adjacent Ferromagnetic-Ferroelectric Heterostructures.* Physical Review Applied, 2017. **7**(1): p. 014013.
40. Qin, H., S.J. Hämäläinen, and S. van Dijken, *Exchange-torque-induced excitation of perpendicular standing spin waves in nanometer-thick YIG films.* Scientific Reports, 2018. **8**(1): p. 5755.
41. Liu, C., et al., *Long-distance propagation of short-wavelength spin waves.* Nature Communications, 2018. **9**(1): p. 738.
42. Klingler, S., et al., *Spin-Torque Excitation of Perpendicular Standing Spin Waves in Coupled YIG/Co Heterostructures.* Physical Review Letters, 2018. **120**(12): p. 127201.
43. Chen, J., et al., *Strong Interlayer Magnon-Magnon Coupling in Magnetic Metal-Insulator Hybrid Nanostructures.* Physical Review Letters, 2018. **120**(21): p. 217202.
44. Li, Y., et al., *Coherent spin pumping in a strongly coupled magnon-magnon hybrid system (to be submitted)*. 2019.